ELSEVIER

Journal of Photochemistry and Photobiology A: Chemistry 145 (2001) 41–47

Journal of Photochemistry and Photobiology A:Chemistry

www.elsevier.com/locate/jphotochem

Femtosecond laser micro-fabrication for tailoring photonic crystals in resins and silica

Vygantas Mizeikis [a], Hong-Bo Sun [a], Andrius Marcinkevičius [a], Junji Nishii [b], Shigeki Matsuo [c], Saulius Juodkazis [c], Hiroaki Misawa [c,*]

[a] *Satellite Venture Business Laboratory, The University of Tokushima, 2-1 Minamijyosanjima, Tokushima 770-8506, Japan*

[b] *Optical Materials Division, Osaka National Research Institute, 1-8-31 Midorigoaka, Iketa, Osaka 563-8577, Japan*

[c] *Department of Ecosystem Engineering, Graduate School of Engineering, The University of Tokushima, 2-1 Minamijyosanjima, Tokushima 770-8506, Japan*

Received 16 April 2001; received in revised form 21 May 2001; accepted 14 June 2001

Abstract

We report laser micro-fabrication of photonic crystal structures in silica glass and photopolymerizing resins, and present a detailed analysis of their structural and optical properties. Photonic crystals with 2D triangular lattice and 3D diamond lattice in glass are found to exhibit moderately pronounced photonic pseudogaps. Formation of planar microcavity is demonstrated in log-pile 3D photonic crystal, laser micro-fabricated in resin.

Keywords: Laser micro-fabrication; Photonic crystal; Photonic bandgap; Silica glass; Photopolymerizing resin

1. Introduction

Fabrication and characterization of photonic crystals (PhC) is one of the current trends in optoelectronics. In PhCs, periodic spatial modulation of dielectric constant leads to formation of allowed photonic energy bands separated by forbidden photonic bandgaps (PBG) for electromagnetic (EM) waves, provided that the modulation amplitude is sufficient, and its period is comparable to the EM wavelength. PhCs exhibiting PBG in the visible and infrared spectral regions are potentially applicable for effective control of light emission and propagation processes. Most PhCs are currently fabricated using semiconductor materials by expensive solid-state technologies matured in microelectronics. Despite many interesting results achieved with these structures, search for simpler and cheaper techniques is underway. In this respect, *femtosecond laser micro-fabrication* [1–3], introduced recently as a tool for structuring of transparent dielectrics, offers interesting possibilities for the PhC fabrication [4,5]. In this work, we report laser micro-fabrication of PhCs with various lattice types in silica glass, and in photopolymerizing resins.

2. Principles and implementation of femtosecond laser micro-fabrication

Fabrication of PhC structures must produce periodic modulation of the refractive index. This usually involves marking and removal of unwanted regions from the initial homogeneous semiconductor, dielectric, or other material. In some cases, ordered arrays of dielectric elements (spheres, bars, etc.) are assembled together into ordered arrays to form a PhC. PBG usually occurs at wavelengths comparable to the PhC period. Hence, to achieve PBG in the visible and infrared spectral regions, features of the PhC must be submicron-sized. This size constraint is the greatest obstacle for cheap and effective fabrication of PhC structures, since the fabrication requires use of sophisticated processing steps (lithography, etching, micromanipulation, etc.).

Laser micro-fabrication is a relatively simple technique, which allows to mark and remove unwanted regions in a few simple processing steps. It is well known that intense light, focused by a lens, can produce burning at the focal spot. Irradiating transparent material with a tightly focused laser beam may produce similar result if the light intensity is sufficient for inducing permanent damage in the material. In some liquid organic pre-polymer solutions, the effect of irradiation by intense light may be solidification. In both cases, photomodification of optical, mechanical, chemical or other properties occur locally at the focal spot of the beam. As far as the PhC fabrication is concerned, it is important to

* Corresponding author. Tel.: +81-88-656-7389; fax: +81-88-656-7598.
E-mail address: misawa@eco.tokushima-u.ac.jp (H. Misawa).

1010-6030/01/$ – see front matter
PII: S1010-6030(01)00565-2

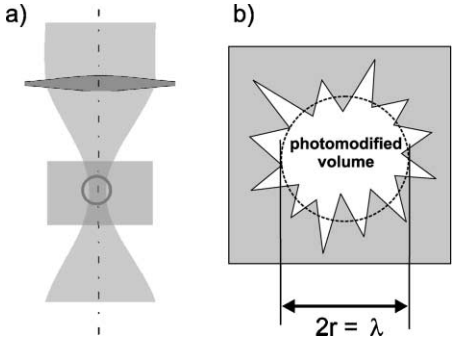

Fig. 1. Laser micro-fabrication by focused laser beams. High power density in the beam waist region (a) creates a photomodified volume in the bulk of transparent initial material (b). Use of high NA microscope objective for tight focusing in conjunction with nonlinear absorption results in photomodified regions comparable to or smaller than diffraction-limited focal spot size.

modify the refractive index in submicron-sized regions by laser irradiation, and to arrange these regions periodically in space.

Fig. 1 describes schematically general features of the laser micro-fabrication process. The laser beam is focused into the interior of a transparent material by a microscope objective. The waist of the beam, where light power density reaches its peak (encircled area in (a) and (b)), defines the location of the photomodified region. The photomodification, which involves a variety of processes, occurs within this region due to the multi-photon absorption. In silica glass, at sufficiently high light intensities the result of the photomodification is a permanent damage, which leaves a tiny cavity in the previously homogeneous glass sample. In resins, photomodification leaves a grain of solid polymerized material inside the liquid sample. The physical processes responsible for the photomodification in both materials will be described in some detail below. The dimensions of the photomodified region depend on the focusing, and may become comparable to the micro-fabricating laser wavelength if microscope objective with a high numeric aperture (NA) is used for the focusing. The initial multi-photon absorption is intensity-dependent, and under certain circumstances, may reduce the photomodified region even below the diffraction-limited focal spot size. The photomodification thus allows to create submicron-sized features with refractive index values different from those in the surrounding regions. Laser micro-fabrication of a PhC structure then involves periodic scanning of the focal spot coordinates, and repeated photomodification at each scanning point.

Experiments reported in this work use pulsed femtosecond ($\tau_{\text{pulse}} \approx 250$ fs) irradiation at the fundamental ($\lambda_{\text{I}} = 795$ nm) or frequency-doubled wavelength ($\lambda_{\text{II}} = 397.5$ nm) of a Ti:Sapphire laser. Samples of purified vitreous silica (EDC from Nippon Glass), and photopolymer Nopcocure 800 (San Nopco) were used as starting materials for the PhC micro-fabrication. In both materials available micro-fabrication wavelengths are in the spectral region below the single-photon absorption edge. To fabricate silica glass, light power density at the focal spot must be sufficient for six-photon (three-photon) absorption using λ_{I} (λ_{II}) pulses. In the case of ultrashort pulse excitation the damage occurs under nonequilibrium conditions. The leading part of the pulse generates free carrier plasma, which in turn enhances the absorption of the trailing part of the pulse, until avalanche ionization is reached. Subsequently, large amounts of the plasma energy become rapidly transferred to the ions of the underlying lattice, heating it and igniting a light-induced microexplosion [6], which leaves an empty voxel (volume element). The voxel has an effective refractive index approaching that of free space ($n = 1$), while the undamaged regions retain their usual value of $n = 1.473$ [2]. Due to the nonlinear nature of the initial absorption process, the damaged region may be somewhat smaller than the focal spot. With high NA microscope objectives, it is realistic to record voxels with radii below 250 nm. Micro-fabrication of resin is performed at the wavelength λ_{II}, at which two-photon absorption is required for the plasma generation. The effect of absorption is to create free radicals by the light-induced bond cleavage, which subsequently triggers the propagation of photopolymerization reaction. The efficiency of this reaction is sensitive to the temperature. Larger temperature at the focus accelerates the polymerization. This renders the exposed regions insoluble, while the unexposed regions can be later removed by dissolving in acetone. It is, therefore, possible to record connected network of photosolidified regions forming self-supporting PhC structures. The refractive index of the solidified resin, $n = 1.49$, is larger than that of air, $n = 1$, thus enabling periodic modulation of the refractive index.

Fig. 2 depicts schematically the experimental set-up used for the micro-fabrication. Laser source is a Ti:Sapphire laser (Tsunami, Spectra Physics) with a regenerative amplifier (Spitfire, Spectra Physics). The micro-fabrication is performed in an optical microscope (Olympus IX-70) with

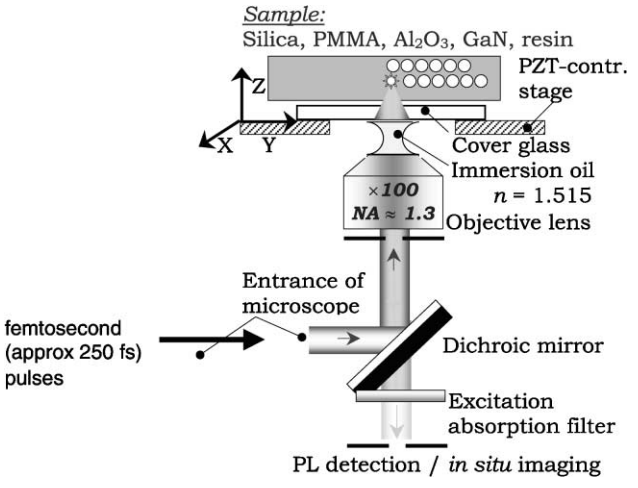

Fig. 2. Sketch of the experimental set-up for laser micro-fabrication of glasses, resins, and other materials.

100× magnification and NA = 1.3–1.35 oil immersion objective lens. Typical lateral and axial spot sizes obtained under tight focusing are $x = 1.22\lambda/\mathrm{NA} \cong 361\,\mathrm{nm}$ and $z = 2n\lambda/\mathrm{NA}^2 \cong 658\,\mathrm{nm}$, where λ is the fabrication wavelength and $n \cong 1.5$ the refractive index at the focal point. The sample, a slab of glass or a drop of liquid resin on a glass substrate, is mounted on a holder attached to a 3D piezoelectric translation stage. The position of the stage is computer-controlled with 50 nm precision. This arrangement, supplemented by a pulse shutter, allows to record practically any 3D patterns of photomodified spots (including periodic patterns). The size of the recorded structures was limited by the maximum range of the piezoelectric translation stage (50 μm × 50 μm × 20 μm).

After the micro-fabrication, the samples were subjected to simple post-processing. In order to improve optical characteristics of glass structures, they were annealed at 700–900°C for 1 h. The annealing improves quality of the PhC structure, because voxels created by micro-explosions are initially somewhat randomly shaped. The improvement is most probably due to the diffusional recovery of the void shell, and leads to a more pronounced PBG transmission dip [5]. The resin samples were washed in acetone in order to dissolve and remove the unexposed regions.

3. Results and discussion

3.1. Photonic crystals in silica

Laser micro-fabrication of 2D and 3D PhCs by coordinate scanning [5,7,8] provides the possibility to realize various types of periodic photonic lattices, also including lattices with defects. Many types of photonic lattices with different dimensionalities and lattice symmetries exist. During the last decade numerous studies have revealed several lattice types, most favorable for opening of the full PBG. Below, we will focus on two promising types of photonic lattices, namely 2D triangular, and 3D diamond.

3.1.1. 2D triangular lattice

Triangular lattice is widely used in 2D PhC devices due to the possibility to achieve wide PBG for a single linear polarization and full PBG for both polarizations. The triangular lattice is described by two primitive translation vectors in the x–y coordinate plane, with equal magnitudes (lattice period a), and mutual orientation of 60°. A PhC with this lattice can be composed from: (i) dielectric rods in air, or (ii) air columns in a dielectric oriented along the z-axis. Laser micro-fabrication of silica glass realizes case (ii) above.

Fig. 3(a) shows the image of laser micro-fabricated 2D PhC with triangular lattice. Periodic PhC structure is evidenced by the bright lines, arranged in a triangular lattice as described above, with $a = 1.2\,\mu\mathrm{m}$. The structure was recorded by multi-shot femtosecond laser irradiation at λ_{II}, by smoothly scanning the coordinate of the irradiated spot along the line direction. Characterization by atomic force microscopy (AFM) has revealed that the bright lines are in fact hollow cylinders with average radius of $r = (0.1\text{–}0.4)a$ [7]. We regard the fabricated structure as a triangular array of air (refractive index $n = 1$) columns in silica ($n_S = 1.473$). Since r is not known precisely, it will be treated as an adjustable variable in the calculations described below.

Transmission along the direction of y-axis may give an indication of the PBG formation. Fig. 3(b) shows the experimental PhC transmission spectra for TE ($\mathbf{E} \perp z$) and

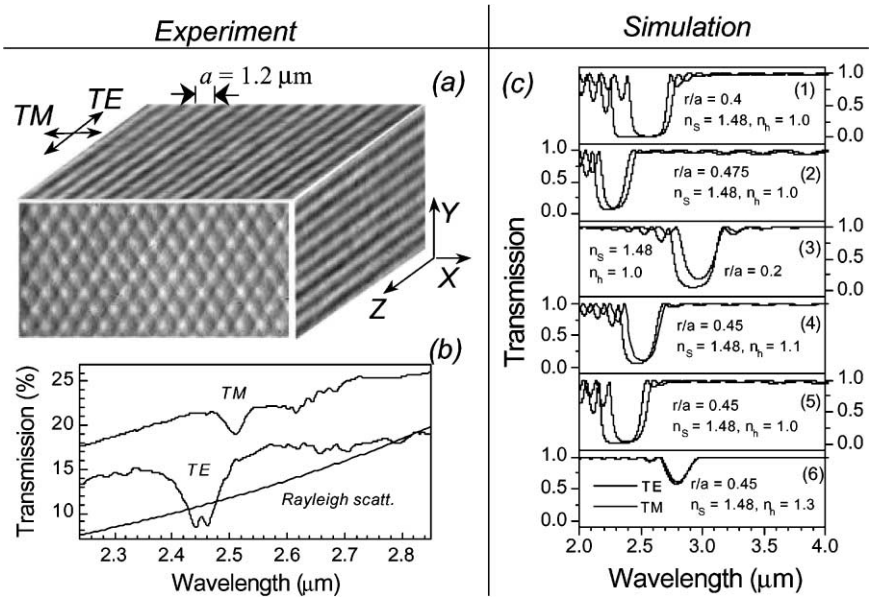

Fig. 3. (a) Reconstructed image of the 2D triangular PhC in silica; (b) FTIR transmission spectra; (c) calculated PhC transmission for TE (black) and TM (gray) linearly polarized light for various n and r/a values.

($\mathbf{E}\|z$) TM waves, measured with a Fourier-transform infrared (FTIR) spectrometer. The transmission dips seen for both polarizations are due to the formation of PBGs. Their fairly small magnitude indicates that the gaps are incomplete. We have calculated the transmission of the idealized model structure with r as an adjustable parameter. The calculations were performed using TransLight software package which utilizes the transfer matrix technique [9]. Fig. 3(c-1) shows the result for $r/a = 0.4$, which is in good qualitative agreement with the experiment. Although the calculated bandgaps are much broader and deeper than the experimental ones, qualitative agreement between the calculated and measured data is satisfactory because: (i) spectral positions for both bandgaps are reproduced fairly well, (ii) small red shift of the TM dip with respect to the TE one is reproduced. The experimentally observed bandgap narrowing and shallowing can be tentatively ascribed to the disorder which is naturally present in structures formed by local microexplosions, where radius, position, and light scattering pattern of each individual "atom" may vary randomly.

To gain better insight into the nature of PBGs, several calculated spectra are presented in Fig. 3(c) for different *r/a* values. As can be seen, increase in the *r/a* ratio leads to the blue shift of both gaps (c-2), while the red shift is obtained with decrease in the *r/a* ratio (c-3). As an alternative to the *r/a* ratio variations, we consider the possibility that only a certain part of the entire micro-fabricated volume within the radius r, subjected to the most intense light illumination during the fabrication, has become hollow, while in the remaining regions the average material (optical) density has decreased towards 0 (the void with $n = 1$). Under these circumstances, we can assign effective values of refractive index n_h ($1 < n_h < n_S$) to the cylindric regions of radius r. Fig. 3(c-4 to c-6) plots the calculated transmission spectra for several values of n_h and fixed $r/a = 0.45$ ratio. The spectrum in Fig. 3(c-4) for $n_h = 1.1$ corresponds well to the experimental data. The following plots (c-5 and c-6) illustrate the effect of n_h on the position and depth of the transmission dip: a decrease in n_h towards 1 (hollow cylinders as in (a)–(c)), leads to the blue shift, while increase in n_h towards n_S results in its red shift and shallowing.

Such behavior can be explained in simple terms as follows [10]. Decrease in *r/a* ratio tends to increase the effective refractive index of the entire PhC volume (including holes), thus decreasing the energies of allowed modes in the crystal, hence causing the red shift. The same effect is obtained when the effective refractive index of the holes is allowed to increase above 1. The peculiar red shift of the TM bandgap with respect to the TE one is a fingerprint of the optical anisotropy in PhC: the TE mode (with electric field perpendicular to the holes) feels stronger discontinuity in n than TM mode (with electric field parallel to the holes). This difference, however, tends to disappear when *r/a* ratio approaches the extreme values 0 and 0.5, or when n_h approaches n_S.

We conclude that the results of calculation shown in Fig. 3(c-1 and c-4) correspond best to the experiments, indicating that the investigated PhC can be with reasonable accuracy described by a 2D triangular lattice of holes with $r/a \approx 0.4$ and effective refractive index $n_h \approx 1.05$ in dielectric with $n = 1.48$. Although both the experiment and calculations predict absence of complete bandgap, use of other materials with a higher refractive index or different lattices (like honeycomb lattice [10]) may improve the results.

3.1.2. 3D diamond lattice

D PhCs with diamond lattice are very attractive due to significantly enhanced PBGs, compared to those in other photonic lattices, including opal. The opal is a prominent type of PhC, ant it is relevant to compare briefly the photonic lattices of opal and diamond-like PhCs. An opal is formed by close-packed arrays of silica nanospheres. Opals were among the first thoroughly investigated PhC structures, because they exist naturally as precious gemstones. Later, high quality artificial opals were synthesized using fairly simple procedure based on self-organized sedimentation from colloidal suspensions [11]. Self-organization leads to the formation of close-packed face-centered cubic (f.c.c.) lattice (see Fig. 4(a)) with the basis of one spherical dielectric atom. It was discovered in the early days of the PhC research that spherical symmetry of the basis tends to suppress the PBG formation [12,13], and that high contrast of refractive index (above 3.5:1) is required to overcome this limitation. Diamond lattice (see Fig. 4(b)) has the same f.c.c. lattice type, but possesses spherically nonsymmetric basis consisting of two atoms, displaced along $\frac{1}{4}$ of the diagonal of the cube. This yields improved PBG properties, and full PBG is likely to open already at the refractive index contrast 2:1. However, diamond lattices cannot be synthesized by self-organization. Laser micro-fabrication provides the versatility, necessary for creating diamond-like PhCs in silica.

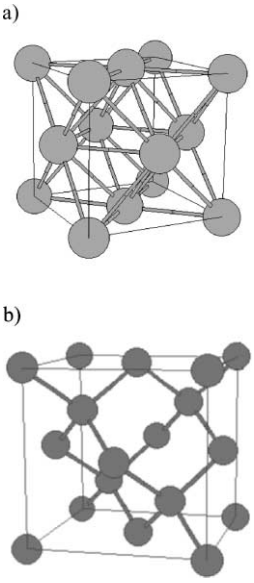

Fig. 4. (a) The f.c.c. lattice with single atom basis, characteristic for opal; (b) f.c.c. lattice with two atom basis, characteristic for diamond.

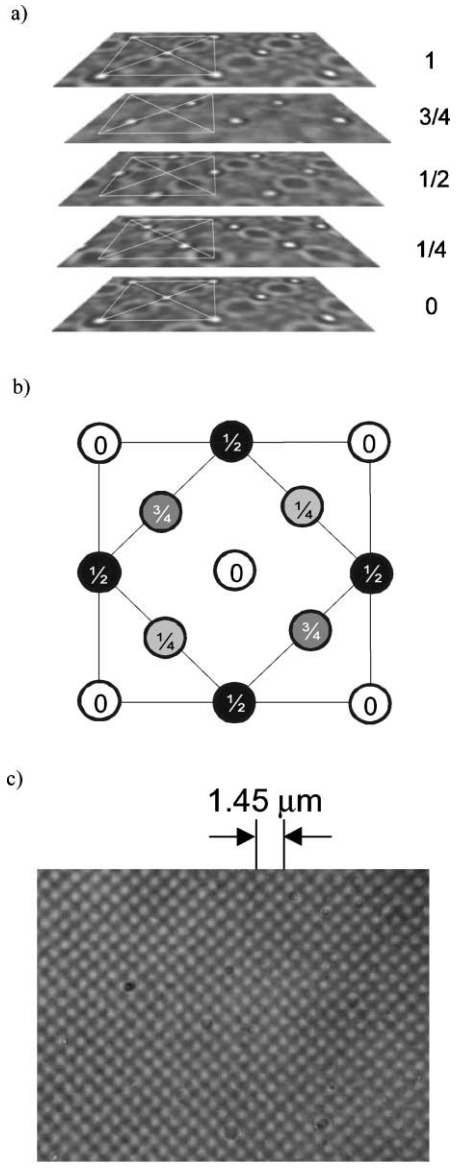

Fig. 5. (a) Optical microscope images of different atomic planes in laser micro-fabricated diamond photonic lattice in glass, relative plane positions are given in the units of lattice period; (b) sketch of atomic arrangement at each atomic plane; (c) optical microscope image of a single plane in the diamond-type PhC with $a = 1.45\,\mu m$.

Fig. 5(a) shows an optical microscopy image of different atomic planes in the laser micro-fabricated diamond PhC with a period of $a = 4\,\mu m$. Schematic explanation of the atomic arrangement of each plane of the diamond lattice is shown in (Fig. 5(b)). The photodamaged regions are again seen as bright spots in the images. The images in Fig. 5(a) are shown for illustration of structural properties of the photonic lattice. Lattice period of this PhC is rather large, and is much larger than the voxel diameter. Hence the PBG would occur in the far infrared spectral range, and due to the small damaged volume, the PBG would be weakly pronounced. A more realistic example of diamond-like PhC with $a = 1.45\,\mu m$ is shown in Fig. 5(c). The image indicates

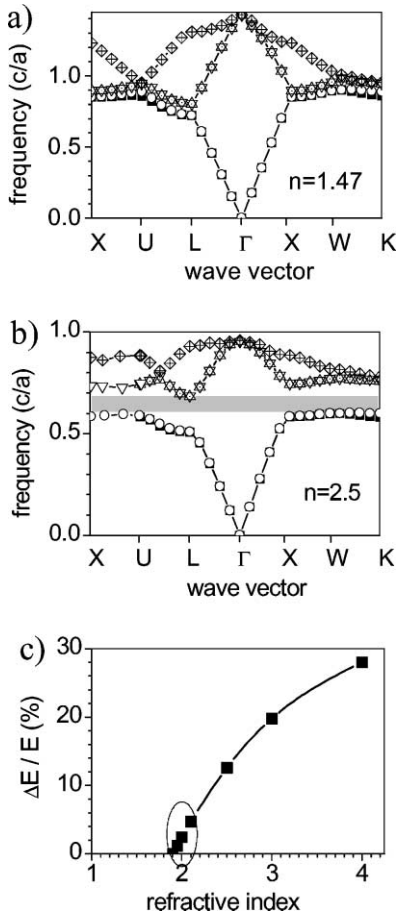

Fig. 6. (a) Photonic band diagram for the PhC structure shown in Fig. 5(c), assuming the refractive index of glass $n = 1.475$; (b) the same assuming $n = 2.5$; (c) the PBG spectral width (in units of PBG center frequency) versus the refractive index of glass. In (a) and (b), frequency axis is calibrated in normalized units of c/a.

structural quality of the PhC at small voxel spacing. The expected PBG spectral position for this PhC falls into the mid-infrared range around 2.5–4 μm (as inferred from calculations). Testing of the PBG properties for this structure was done by calculating its photonic band diagram. The calculations were performed by iterative eigenvalue solver technique, taking the glass refractive index $n = 1.47$ the lattice period $a = 1.45\,\mu m$, and the voxel radius $r = 0.3a$. The results are shown in Fig. 6. As can be seen from the plot in Fig. 6(a), full PBG is absent for these lattice and glass parameters. For comparison, we present the photonic band diagram of similar lattice recorded in glass with higher refractive index $n = 2.5$. In this case, full PBG is clearly visible between the second and the third bands (indicated by the rectangular region in Fig. 6(b)). More detailed examination of the PBG width versus the refractive index of the glass (Fig. 6(c)) indicates that photonic pseudogap evolves into a full gap at $n \approx 1.95$, so it would be necessary to use glass or other material with refractive index corresponding to the region marked by the oval in Fig. 6(c). Some enhancement of the PBG can be also achieved by increasing the voxel radius

(this can be done by increasing the intensity of the fabricating beam), but in this case voxels may become too close to each other, making the structure mechanically unstable. In spite of the absence of PBG in the fabricated structure, laser micro-fabricated diamond PhCs remain highly promising if glass (or other material suitable for laser micro-fabrication) with refractive index close to 2 will become available.

3.2. Photonic crystals in resins

Using smooth scanning of the focal point coordinates, PhCs were fabricated in Nopcocure 800 resin with λ_{II} laser pulses. Examples of the fabricated PhC structures with various dimensionalities are shown in Fig. 7(a). In contrast to PhCs in silica glass where adjacent structural elements must not connect, photosolidified regions in resin must be interconnected to ensure the mechanical stability. Drawing of continuous lines during the fabrication was done by smoothly translating the sample, such that the neighboring laser shots overlap spatially by more than 99%.

The 3D structure depicted in Fig. 7(a-3) is a widely studied log-pile type structure (see Fig. 8(a) and (b) for a schematic and large scale views, respectively). Log-pile type PhCs were previously fabricated using various techniques and from various starting materials. Space lattice of the log-pile has f.c.c. tetragonal symmetry, and favors large photonic bandgaps. The measured optical transmission of the samples with different lattice periods is shown in Fig. 7(b) [4]. Red shift of the transmission dips with increasing distance between the rods clearly indicates PBG effects in this structure. The transmission does not vanish in the gap region, hence PBGs are incomplete. The most likely reason for this is relatively low refractive index contrast.

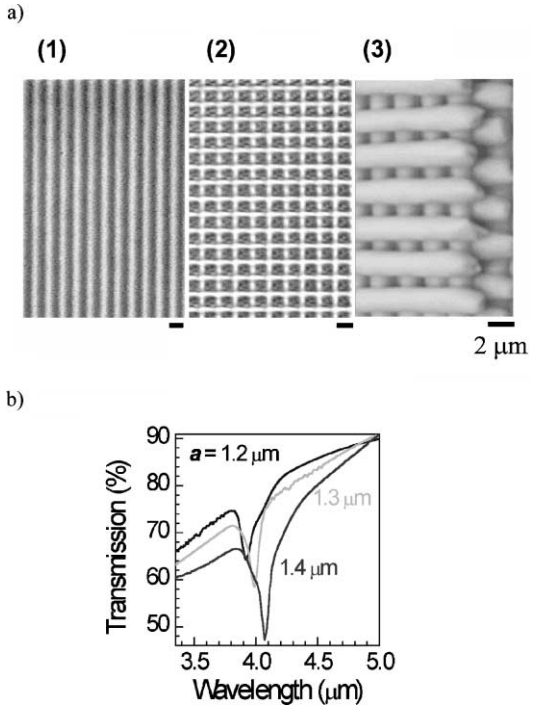

Fig. 7. (a) 1D, 2D and 3D structures fabricated in Nopcocure 800 resin; (b) optical transmission of the PhC structure in (a-3) for different distances between the rods $a = 1.4$, 1.3, 1.2 μm. Images (a-1) and (a-2) are optical transmission images, while (a-3) is the scanning electron microscopy image.

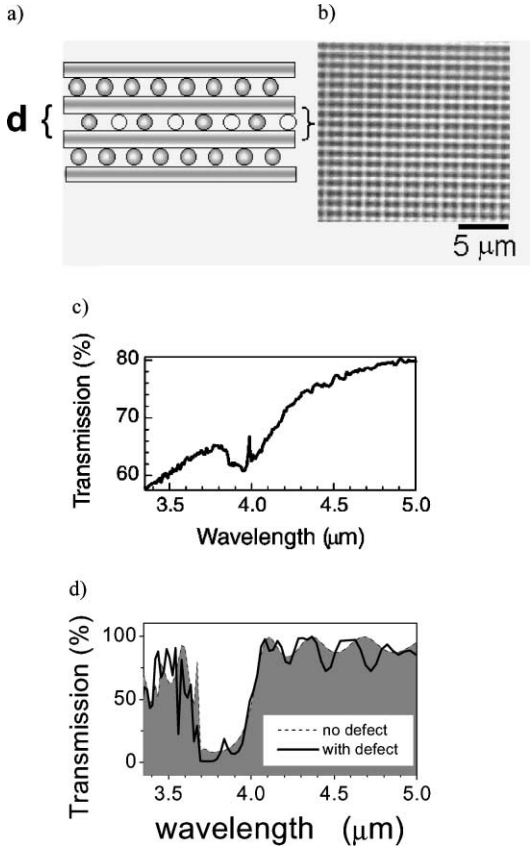

Fig. 8. (a) Sketch of a log-pile PhC structure with planar defect, missing rods are marked by dashed lines; (b) optical microscopy image of the structure; (c) measured transmission spectra of the sample (solid line), and of the reference sample without defects (dashed line); (d) simulated transmission spectra with defects (solid line), and without defects (dashed line with drop-down shadow).

Despite this deficiency, PBG effects in the log-pile PhC are sufficiently strong for the formation of planar microcavities (MC). A planar MC can be created in a log-pile PhC by introducing one or more planar defects in the middle. To test this possibility, we have fabricated log-pile structure with total number of 20 layers, and every other rod missing in the 10th layer. This was accomplished by simply closing the laser beam while drawing particular lines. Fig. 8(a) depicts schematically the middle part of the log-pile PhC with planar defect introduced as described above. It is relevant to note here that defects can be also introduced by adding extra rods, changing their periodicity, orientation angle or diameter (by adjusting the laser pulse energy). The rod diameter in the PhC was $2r \approx 0.8$ μm (assuming cylindric rod shape), the in-plane distance $d \approx 1.3$ μm, and the rod length $l \approx 40$ μm. Fig. 8(b) shows optical microscopy image of the

structure (top view), which evidences high structural quality of the sample.

Fig. 8(c) shows optical transmission spectra of the investigated sample with defect for unpolarized light propagating along the layer stacking direction ⟨0 0 1⟩. It is relevant to compare this spectrum with that shown in Fig. 7(d) for $d \approx 1.3\,\mu m$ in the defect-free sample, which can be used as a reference. The pronounced transmission dips seen around 4.0 μm are signatures of photonic pseudogaps. Transmission spectrum of the sample with defect also reveals evolving defect modes, evidenced by a peak within the transmission dip. Physical origin of the peak can be roughly explained in terms of multiple reflections of light between two PBG mirrors surrounding the defect layer, and forming a planar microcavity. Hence, the peak marks the formation of the microcavity resonance. From the transmission data, we have estimated the quality factor of the cavity $Q \approx 130$. It is helpful to note here that this factor is still somewhat lower than that found in high quality planar semiconductor microcavities. Such relatively low Q means that the planar defect exerts a localizing perturbation on the light modes at the mid-gap, but their spatial spreading and escape from the defect region is also significant, and may even exceed the geometric volume of the defect. Formation of the PBG and microcavity resonance was also confirmed by the numeric modeling. Fig. 8(d) shows the transmission spectra of the reference sample and the sample with defect, calculated using the transfer matrix technique. A model structure shown in Fig. 8(a) with $r = 0.4\,\mu m$, $d = 1.3\,\mu m$, and refractive index of rods $n = 1.6$ was used for the calculations. The calculations qualitatively reproduce the measured transmission spectra by yielding correct spectral positions of PBG-related transmission dips and the defect peak. Detailed analysis and characterization of laser micro-fabricated polymeric microcavities will be published elsewhere [14]. Manifestation of the defect states is, to the best of our knowledge, the first such observation in resin-based PhC [1].

4. Conclusions

Femtosecond laser micro-fabrication provides numerous advantages for the fabrication of PhCs in resins, silica, and possibly other materials. PhCs with arbitrary lattice structure and defect arrangement can be relatively easily and inexpensively fabricated by this technique. Formation of PBG and defect states in the laser micro-fabricated structures was demonstrated experimentally and reproduced by numeric simulations in agreement with the experimental data. Despite current deficiencies which prevent realization of full photonic bandgaps in laser micro-fabricated PhC, potential possibilities of laser micro-fabrication are high, and are likely to evolve significantly in the near future.

Acknowledgements

This work was supported in part by a grant-in-aid for Scientific Research (A)(2) from the Japanese Ministry of Education, Science, Sports and Culture (09355008), the Marubun Research Promotion Foundation, and Satellite Venture Business Laboratory of the University of Tokushima.

References

[1] H. Misawa, S. Juodkazis, H. Sun, S. Matsuo, J. Nishii, in: Proceedings of the Laser Precision Micro-fabrication, LPM2000, Vol. 4088, SPIE, 2000, pp. 29–32.
[2] H. Misawa, H. Sun, S. Juodkazis, M. Watanabe, S. Matsuo, in: H. Helvajian, K. Sugioka, M.C. Gower, J.J. Dubowski (Eds.), Laser Applications in Microelectronic and Optoelectronic Manufacturing V, Vol. 3933, SPIE, 2000, pp. 246–260.
[3] H. Misawa, S. Juodkazis, A. Marcinkevičius, V. Mizeikis, A. Yamaguchi, H. Sun, S. Matsuo, in: Proceedings of the International Symposium on Micromechatronics and Human Science, Nagoya, Japan, October 22–25 (2000) 23.
[4] H. Sun, S. Matsuo, H. Misawa, Appl. Phys. Lett. 74 (1998) 786.
[5] H. Sun, Y. Xu, K. Sun, S. Juodkazis, M. Watanabe, S. Matsuo, H. Misawa, J. Nishii, in: Proceedings of the MRS Fall Meeting'99, Vol. 605, Materials Research Society, 2000, pp. 85–90.
[6] M. Watanabe, S. Juodkazis, S. Matsuo, J. Nishii, H. Misawa, Jpn. J. Appl. Phys. 39 (2000) 6763.
[7] H. Sun, Y. Xu, S. Juodkazis, K. Sun, J. Nishii, Y. Suzuki, S. Matsuo, H. Misawa, in: X. Chen, T. Fujioka, A. Matsunawa (Eds.), Proceedings of the High-power Lasers in Manufacturing, Vol. 3888, SPIE, 2000, pp. 131–142.
[8] H. Sun, Y. Xu, S. Matsuo, H. Misawa, Opt. Rev. 6 (1999) 396.
[9] A.L. Reynolds, TransLight software, for detailed description of the program and algorithm of calculations, see http://www.elec.gla.ac.uk/~areynolds/Software/Software-Main.html.
[10] J.D. Joannopulos, R.D. Meade, J.N. Winn, Photonic Crystals: Molding the Flow of Light, Princeton University Press, Princeton, NJ, 1995.
[11] H. Miguez, C. López, F. Meseguer, A. Blanco, L. Vásquez, R. Mayoral, Appl. Phys. Lett. 71 (1996) 1148.
[12] K. Ho, C. Chan, C. Sokoulis, Phys. Rev. Lett. 65 (1990) 3152.
[13] E. Yablonovitch, T.J. Gmitter, K.M. Leung, Phys. Rev. Lett. 67 (1991) 2295.
[14] H.-B. Sun, V. Mizeikis, Y. Xu, S. Juodkazis, J.-Y. Ye, S. Matsuo, H. Misawa, Appl. Phys. Lett. 79 (2001) 1.